Supramolecular association of halochromic switches and halloysite nanotubes into fluorescent nanoprobes for intracellular detection

Marina Massaro,[a,1] Monica Notarbartolo,[a,1] Françisco M. Raymo,[b,*] Giuseppe Cavallaro,[c,d] Giuseppe Lazzara,[c,d] Mercedes M. A. Mazza,[b] Cesar Viseras-Iborra[e,f] and Serena Riela[a,*]

[a]*Dipartimento di Scienze Biologiche, Chimiche e Farmaceutiche (STEBICEF), University of Palermo Viale delle Scienze, 90128 Palermo, Italy.*

[d]*Laboratory for Molecular Photonics, Department of Chemistry, University of Miami,1301 Memorial Drive, Coral Gables, FL 33146-0431.*

[c]*Dipartimento di Fisica e Chimica "E. Segrè (DiFC), University of Palermo, Viale delle Scienze, 90128 Palermo, Italy.*

[d]*Consorzio Interuniversitario Nazionale per la Scienza e Tecnologia dei Materiali, INSTM, I-50121 Firenze, Italy.*

[e]*Department of Pharmacy and Pharmaceutical Technology, Faculty of Pharmacy, University of Granada, Campus of Cartuja, 18071 s/n, Granada, Spain.*

[f]*Andalusian Institute of Earth Sciences, CSIC-UGR, Avenida de las Palmeras 4, 18100, Armilla, Granada, Spain.*

[1]Contributed equally

KEYWORDS. Halloysite nanotubes, halochromic switches, fluorescent probes, intracellular detection.

ABSTRACT. Fluorescence imaging has become an indispensable tool in the biomedical laboratory to elucidate the fundamental dynamic and structural factors regulating cellular processes. The development of fluorescent nanoprobes represent a challenge to detect any cellular process under the microscope. Herein, a novel fluorescent nanomaterial was synthetized by exploiting the supramolecular interaction between a halochromic switch (**1Cl**) and halloysite nanotubes (HNTs). The obtained HNTs/**1Cl** nanomaterial was thoroughly studied by FT-IR and thermogravimetric analyses and the aqueous mobility was investigated by dynamic light scattering (DLS) and ζ–potential measurements. Furthermore, the morphology was imaged by transmission electron microscopy (TEM) and the interaction of the clay with the **1Cl** was also studied by kinetic adsorption measurements. In addition, the spectroscopy properties of the resulting nanomaterial were studied in solution and in the solid state by UV-*vis* and fluorescence measurements. Finally, the ability of our nanomaterial to detect cancer cells was assessed with confocal laser-scanning microscopy measurements on normal (hTERT) and/or tumoral cell lines (MCF-7 and HL-60R).

INTRODUCTION. The early detection of cancer is a decisive factor to fight this disease. Nanotechnology has been employed in the design of nanomaterials able to overcome biological barriers that also possess intrinsic properties suitable for cancer diagnosis.

Fluorescence imaging has become an indispensable tool in the biomedical laboratory to elucidate the fundamental dynamic and structural factors regulating cellular processes.[1] Indeed, the fast response and high sensitivity of fluorescence measurements,[2] together with the spatial resolution

of optical microscopes,[3] permit the visualization of subcellular structures in real time. A given sample of interest, however, must first be labeled with appropriate emissive probes for a fluorescence image to be captured. Excitation wavelengths causing minimal autofluorescence from and photodamage to the biological sample, small physical dimensions ensuring negligible structural perturbation to subcellular structures as well as sufficient aqueous solubility for administration to the extracellular matrix are generally the main characteristics expected from fluorescent probes for cellular imaging.[4]

Nonetheless, most organic chromophores are relatively hydrophobic and the latter requirement (*i.e.*, aqueous compatibility) demands the covalent incorporation of hydrophilic groups with appropriate synthetic modifications. Alternatively, noncovalent encapsulation of hydrophobic fluorophores in supramolecular carriers can be exploited to solubilize the emissive probes in aqueous media, transport them across the plasma membrane of target cells and deliver them into selected intracellular compartments.[5]

Halloysite nanotubes (HNTs), a natural clay belonging to the kaolin group, have attracted attention for application in bioimaging.[6] HNTs, an aluminosilicate with a chemical formula of $Al_2Si_2O_5(OH)_4 \cdot nH_2O$, consist of rolled kaolinite sheets, where siloxane groups are localized at the external surface and aluminum hydroxide ones are present in the lumen. Generally, the inner and outer diameters of the tubes are in the ranges of 10–30 nm and 40–70 nm, respectively, while their length is in the range of 0.2–1.5 μm. Halloysite possesses different charged surfaces: positive in the inner lumen; negative in the external one, resulting in a significant influence on the aggregation and dispersion of HNTs in aqueous media. The modification of the inner and/or outer surfaces opens different strategies to improve HNTs properties expanding the application fields.

Halloysite biological safety was reported both by *in vitro* and *in vivo* studies.[7] HNTs can penetrate the cellular membrane surrounding the cell nuclei.[8] In addition, it was demonstrated that the modification of the tubes surfaces makes hybrid nanomaterials that penetrate the nucleus membrane, as well.[9]

Recently, it was reported the loading of fluorescent dyes into HNTs lumen or on the external surface and it was demonstrated that the presence of halloysite increases the dyes solubility in physiological conditions and improves its physico-chemical properties. Therefore nanomaterials based on HNTs could be useful for application in bio-imaging field.[8b, 10]

Herein, we report a study of the interaction between a halochromic switch and HNTs as probe for tumor detection. To reach this goal, a fluorescent coumarin chromophore combined with a switchable oxazine (compound **1Cl**) was chosen as model.[11] Upon acidification, the oxazine ring opens to generate **1OpH** (Figure 1).[12] This structural transformation brings the coumarin chromophore in electronic conjugation with the 3*H*-indolium cation to shift bathochromically its absorption and emission bands. As a result, intense fluorescence in the red region of the electromagnetic spectrum appears only after stimulation of **1Cl** with acid inputs. On the basis of this behavior, we were able to acquire images of fixed cells with subdiffraction resolution[13] as well as highlight acidic organelles of live cells.[14] However, this relatively hydrophobic and water-insoluble compound (*i.e.*, **1Cl**) had to be encapsulated noncovalently within polymer nanoparticles[13a] or connected covalently to amphiphilic polymers[14] or secondary antibodies[13b] to be delivered to intracellular targets.

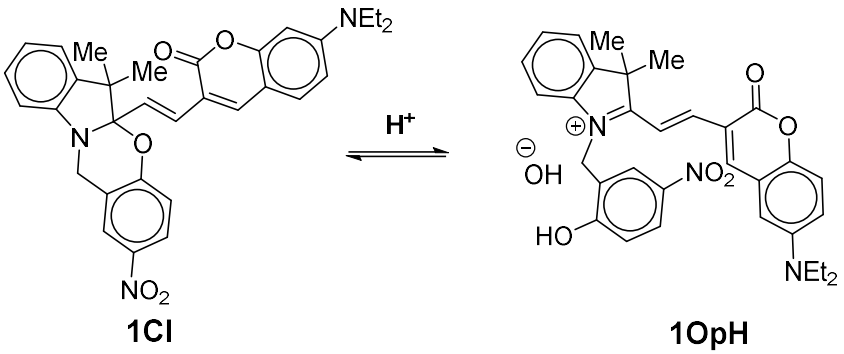

1Cl **1OpH**

Figure 1. Reversible interconversion of **1Cl** and **1OpH**.

On the basis of these considerations, we envisaged the possibility of solubilizing **1Cl** in aqueous media, under the supramolecular assistance of HNTs, with the ultimate objective of transporting this pH sensitive fluorophore into the intracellular environment.

The obtained HNTs/**1Cl** nanomaterial was thoroughly studied by FT-IR and thermogravimetric investigations and the aqueous mobility was investigated by dynamic light scattering (DLS) and ζ–potential measurements. Furthermore, the morphology was imaged by transmission electron microscopy (TEM) and the interaction of the clay with the halochromic switch was also studied by kinetic adsorption measurements. In addition, the spectroscopy properties of the resulting nanomaterial were studied in solution and in the solid state by UV-*vis* and fluorescence measurements.

Finally, the ability of our nanomaterial to detect cancer cells was assessed with confocal laser-scanning microscopy measurements on normal (hTERT) and/or tumoral cell lines (MCF-7 and HL-60R).

MATERIALS AND METHODS.

Halloysite nanotubes used in this study were obtained from Merck and used as received. **1Cl** was synthetized as reported elsewhere.[14]

Thermogravimetric analyses were performed on a Q5000 IR apparatus (TA Instruments) under a nitrogen flow of 25 cm^3 min^{-1} for the sample and 10 cm^3 min^{-1} for the balance. The weight of each sample was ca. 10 mg. Measurements were carried out by heating the sample from room temperature up to 900 °C at a rate of 10 °C min^{-1}.

FTIR spectra (KBr) were recorded with an Agilent Technologies Cary 630 FT-IR spectrometer. Specimens for these measurements were prepared by mixing 5 mg of the sample powder with 100 mg of KBr.

UV-*vis* measurements were performed using a Beckmann DU 650 spectrometer.

Steady-state fluorescence spectra were acquired using a JASCO FP-777W spectrofluorometer. Excitation and emission slits were 1.5 and 3 nm, respectively, with an emission interval ranging between 400 and 800 nm.

Dynamic light scattering (DLS) measurements were carried out by means of a Zetasizer NANO-ZS (Malvern Instruments). The field-time autocorrelation functions were fitted by Laplace transformation, which provided an intensity-weighted apparent hydrodynamic radius (R_h). In detail, the fitting of the field-time autocorrelation functions provided the decay rate (Γ) of the diffusive mode. For the translational motion, the collective diffusion coefficient at a given concentration is $D_t = \Gamma/q^2$ where q is the scattering vector given by $4\pi n\lambda^{-1} \sin(\theta/2)$, with *n* being the water refractive index, λ the wavelength (632.8 nm), and θ the scattering angle (173°). The apparent hydrodynamic radii were calculated by using the Stokes−Einstein equation as $R_h = k_bT/(6\pi\eta)$, k_b being the Boltzmann constant, T the absolute temperature, and η the water viscosity.

ζ–potential measurements were carried out by means of a Zetasizer NANO-ZS (Malvern Instruments) at 25.0 ± 0.1 °C. The concentration of the dispersions was 10^{-3} wt%.

Transmission electron microscopy (TEM) was performed by means of a FEI Titan G2 60–300 ultra-high-resolution transmission electron microscope (FEI, Lausanne, Switzerland) coupled with analytical electron microscopy (AEM) performed with a SUPER X silicon drift windowless energy dispersive X-ray spectroscopy (XEDS) detector. AEM spectra were saved in mode STEM (scanning transmission electron microscopy) with a HAADF (high angle annular dark field) detector.

Adsorption kinetics

The batch experiments were carried out for investigating the adsorption kinetics of **1** onto HNTs at room temperature in water. For the experiment, HNTs (1 ± 0.5 mg) were added into 2 mL of water and after, 0.5 mL of **1** solution in acetonitrile (1×10^{-4} M) were added. The amount of **1** adsorbed at time *t* (Q_t, mol g^{-1}) was calculated by the following equation:

$$Q_t = \frac{(C_0 - C_t) \cdot V}{M} \qquad \text{(Eq. 1)}$$

where C_0 and C_t are initial and *t* time concentrations of **1** (M), respectively, *M* is the weight of HNTs (g) and *V* is the volume of **1** solution (L).

Kinetic Release

The release of **1** from the HNT was done as follows: 10 mg of the sample were dispersed in 0.5 mL of dissolution medium and transferred into a dialysis membrane (Medicell International Ltd MWCO 12-14000 with a diameter of 21.5 mm). Phosphate buffer (0.05 M, pH 7.4) was used as the release medium. Subsequently the membrane was put in a round bottom flask containing 5 mL of the release medium at 37 °C and stirred. At fixed time, 1 mL of the release medium has been withdrawn and analyzed by UV-*vis* measurements. To keep constant the volume of the

release medium, 1 mL of fresh solution has been used to replace the collected one. Total amounts of drug released (F_t) were calculated as follows:

$$F_t = V_m C_t + \sum_{i=0}^{t-1} V_a C_i \qquad \text{(Eq. 2)}$$

where V_m and C_t are the volume and the concentration of the drug at time t. V_a is the volume of the sample withdrawn and C_i is the drug concentration at time i ($i < t$).

Confocal images were acquired with an Olympus FluoView10i confocal laser scanning microscope (Olympus, Japan) equipped with humidity control and CO_2 using a 10 × 0.3 NA objective. Aliquots of HNTs/**1** dispersed in water were deposited on a cover glass (BRAND #1) using a disposable pipette. Measurement was acquired using laser excitation at 405 nm or 595 nm. Emitted fluorescence was acquired in photon-counting mode. Spectral detection has been performed using a bandwidth of 5 nm and a step size of 3 nm in the range 420–740 nm. The scan area was 256 × 256 pixels and the scan speed was 12 µs per pixel.

RESULTS AND DISCUSSION

The loading of **1Cl** into halloysite was carried out by mixing an aqueous dispersion of halloysite (5 mL) with a concentrated **1Cl** solution in ACN (10^{-2} M, 1 mL) (Scheme 1). Then, the obtained suspension was stirred and maintained under vacuum for 3 to 5 min, resulting in light fizzling, which indicated that air was released from the tubes.

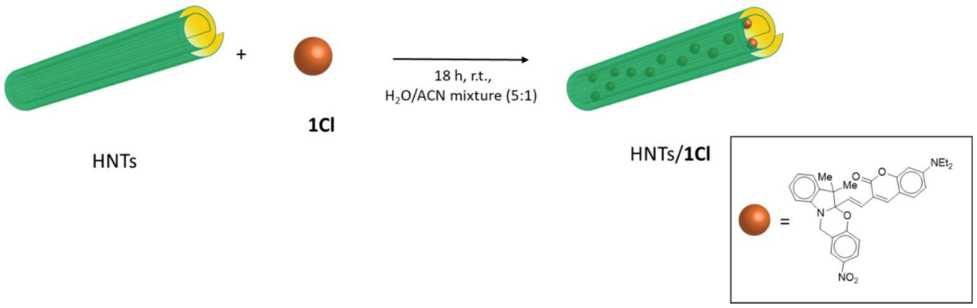

Scheme 1. Schematic representation of the synthesis of HNTs/**1Cl** nanomaterial.

Once the vacuum was removed, the solution entered the lumen and the loaded compound adsorbed within the tubes. This procedure was repeated 2 to 3 times to improve the loading efficiency.

The dye loading of HNTs/**1Cl** was estimated by UV-*vis* spectroscopy. The amount of **1Cl** loaded in the HNTs, expressed as the percent amount of dye in the final nanomaterial, was *ca.* 6 wt% with an entrapment efficiency of 95%.

The HNTs/**1Cl** nanomaterial was characterized by FT-IR spectroscopy, thermogravimetric analysis and the colloidal properties were estimated by dynamic light scattering and ζ–potential measurements. Furthermore, the morphology of the nanomaterial was imaged by transmission electron microscopy (TEM) and High Angle Annular Dark Field Scanning TEM (HAADF-STEM).

In Figure 2a, the FT-IR spectra of HNTs/**1Cl** nanomaterial and the pristine components HNTs and **1Cl** are reported. The assignments for the bands of the pristine halloysite can be done on the basis of literature data.[15] The FT-IR spectrum of **1Cl** shows the bands at 2966, 2927 and 2848 cm^{-1} corresponding to asymmetric and symmetric stretching of the methyl and methylene groups, the characteristic band 1714 cm^{-1} ascribed to the C=O group and the bands between 1620 and 900 cm^{-1} derive from stretching and bending of aromatic ring and C—O, C—N stretching

vibrations. All these characteristic bands are present in the FT-IR spectrum of HNTs/**1Cl**, providing direct evidence of the successful loading of **1Cl** into HNTs.

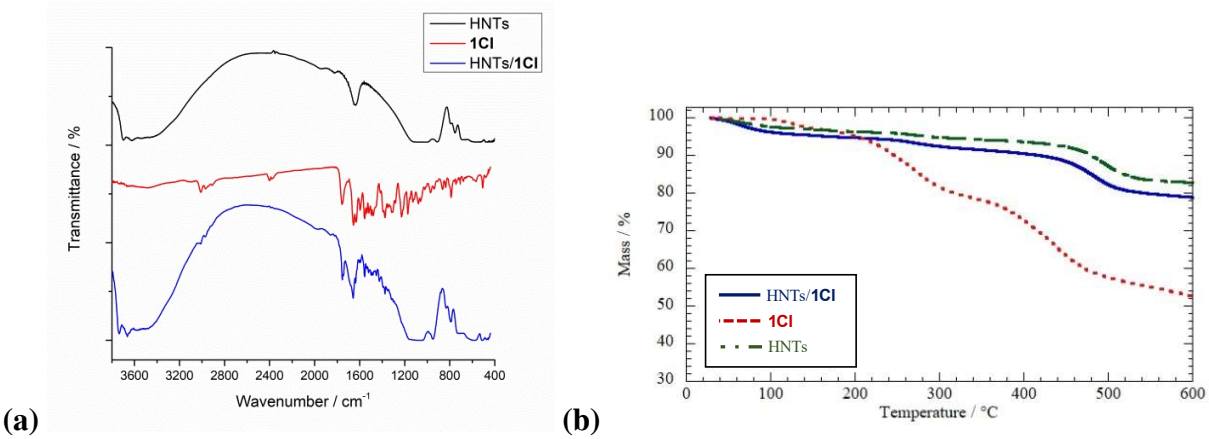

Figure 2. (a) FT-IR spectra and (b) thermogravimetric curves of **1Cl**, HNTs and HNTs/**1Cl** nanomaterial.

Figure 2b shows the thermogravimetric curves of HNTs/**1Cl** and its pristine components (HNTs and molecule **1Cl**).

As reported in our previous studies,[15-16] we estimated the functionalization efficiency of HNTs surfaces through the rule of mixtures by considering the residual masses at 600 °C and taking into account the water contents, which were determined by the mass losses between 25 and 150 °C. Accordingly, we calculated that the loading of the molecule **1Cl** in the HNTs/**1Cl** nanomaterial is 7.0 ± 0.4 wt% in agreement with UV-*vis* measurements.

TEM and HAADF-STEM images showed that the structure of HNTs (Figure 3a-b) was preserved after **1Cl** loading. The nanomaterial indeed, exhibits the characteristic hollow tubular structure of halloysite. Energy Dispersive X-ray Spectroscopy (EDS) elemental mapping showed that the **1Cl** molecules are present on the overall surface of the tubes, as highlighted by the distribution of N atoms (Figure 3c). Moreover, close observation of the tubes (Figure 3d) showed the presence of N atoms co-localized both on the external surface and in the lumen as proved by

the EDS elemental mapping performed along HNTs section (selected area in green). These findings led us to hypothesize that the interaction of **1Cl** with HNTs occurs on both surfaces.

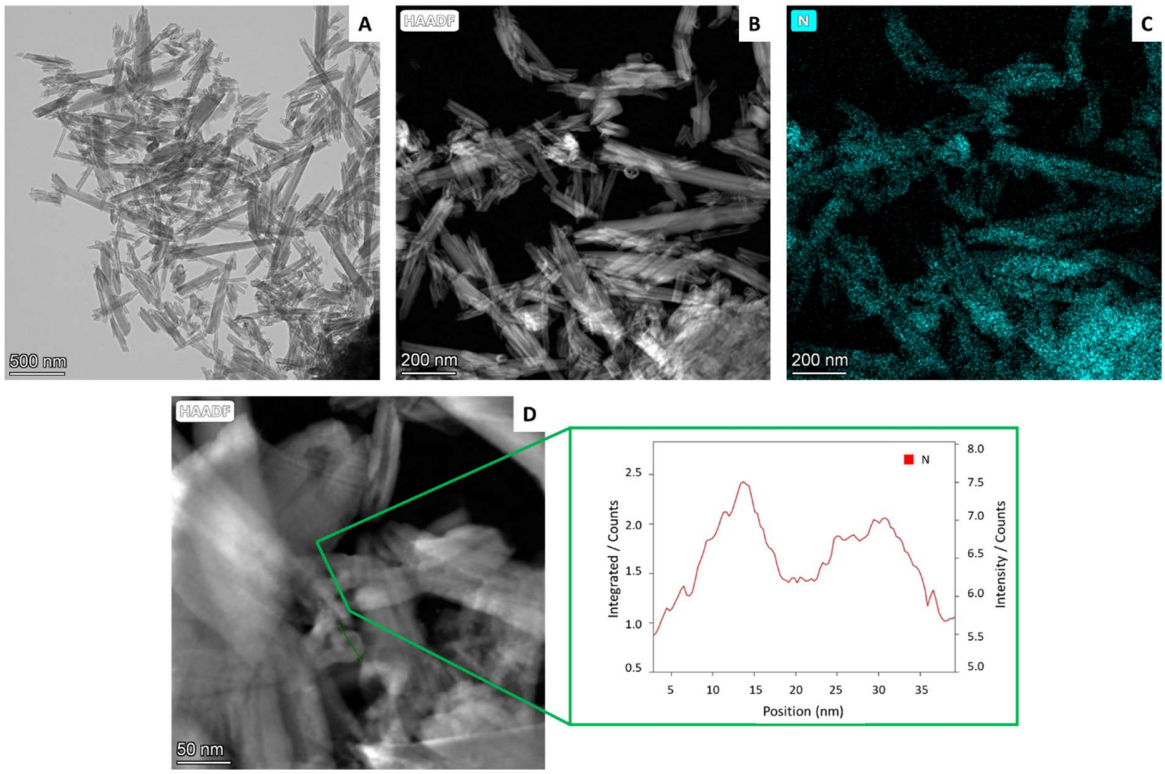

Figure 3. (a) TEM and (b) HAADF/STEM images of HNTs/**1Cl** nanomaterial, (c) EDX elemental mapping image; (d) esteem by EDS elemental mapping of N atoms along the selected area of HAADF/STEM image of HNTs/**1Cl** nanomaterial.

The structural characteristics of HNTs/**1Cl** nanomaterial were investigated by monitoring its mobility in water through DLS measurements.

By this technique, indeed, it was possible to calculate the average translational diffusion coefficient which is related to the dimension and shape of the diffusing particles, their hydration, solvent viscosity, and aggregation phenomena. HNTs are anisotropic objects with a high aspect ratio, which can change due to functionalization. Moreover, the particles ability to interact and aggregate can also depend on surface decoration. Thus, a detailed quantitative analysis of the

results was hampered. Valuable information was achieved by using the Stokes-Einstein equation to calculate the average diameter of the equivalent sphere, which can be considered as an index to follow the changes in particle dimensions and intra-particle aggregation.

The intensity-weighted diffusion coefficient distribution of HNTs/**1Cl** showed a monomodal distribution with the peak centered at 5×10^{-13} m^2 s^{-1}, that corresponds to a hydrodynamic diameter of 437 nm. This value is close to that of pure HNTs[15] indicating that the aqueous dynamic behavior of the HNTs/**1Cl** hybrid reflects that of single halloysite nanotubes. On this basis, we can conclude that HNTs/**1Cl** does not present any clustering processes.

As concerns the surface charge, the HNTs/**1** nanomaterial presents a negative ζ-potential (-24.8 ± 0.8 mV). It should be noted that the net charge of the nanotubes was slightly increased by the functionalization with **1Cl**, being that the ζ-potential of pristine halloysite is -21 mV.[17]

To shed some light on the interaction of **1Cl** with HNTs we perform some kinetic adsorption experiments. Compound **1Cl** can convert into its protonated open form (**1OpH**), in the presence of water, following the opening of the oxazine ring (Figure 1) at room temperature. This structural modification extends the electronic conjugation of the coumarin fragment over the adjacent 3*H*-indolium cation and shifts its main absorption bathochromically by more than 160 nm with a concomitant change in color.[14] The UV-*vis* spectrum of a solution (in a mixture H_2O/ACN 4:1) of **1Cl** and **1OpH** showed therefore two different absorption maxima related to the two different **1** forms. By adding HNTs to a solution (in a mixture H_2O/ACN 4:1) of **1** (**1Cl** and **1OpH** forms) and recording the UV-*vis* spectra of the supernatant solution over time, it was found that only the maximum at λ_{abs} 410 nm was affected by the presence of HNTs (Figure S1a). Under the same conditions, the UV-*vis* spectrum of **1**, in the absence of HNTs, did not show any

changes (Figure S1b). This finding led us to hypothesize that **1Cl** is selectively adsorbed into the tubes.

Since the ring-open isomer is predominantly converted into the protonated form (**1OpH)** in aqueous medium, the observed selectivity could be ascribed to the low affinity of **1OpH** for the positively charged HNTs lumen and therefore the interaction is mainly with the **1Cl** isomer.

To better understand the adsorption mechanisms, kinetic of **1Cl** adsorption onto HNTs, in aqueous solution, was investigated (Figure S2). It was found that the adsorption amount increases rapidly in the first 50 min and then slows until the sorption reached equilibrium. As the surface-active sites are occupied, the adsorption rates slow down and finally reach the adsorption equilibrium.

The kinetic data were fitted by first-order, second-order, intra-particle diffusion, and double exponential (DEM) models. It was found that the experimental data are better fitted by the DEM model. According to the literature, the DEM mode describes a process where the adsorbent offers two different types of adsorption sites. Therefore, it could be possible that rapid adsorption equilibration occurs within a few minutes onto the HNTs external surface (k_1 = 0.13 ± 0.02 min^{-1}), whereas on the HNTs lumen, adsorption occurs more slowly (k_2 = 0.0030 ± 0.0005 min^{-1}). The latter result is in agreement with morphological investigations.

To verify the absence of leaching of the dye from the HNTs lumen, we performed a preliminary investigation to study the kinetic release of compound **1Cl** in physiological medium.

The release of **1Cl** loaded in HNT was evaluated by the dialysis bag method using conditions designed to mimic physiological conditions (phosphate buffer pH 7.4). In these conditions only ca. 12 wt% of the total amount of **1Cl** loaded into HNTs was released within 24 h indicating that negligible leaching occurs (Figure 4). Noteworthy, under these conditions the absorption

spectrum of **1Cl** released shows the characteristic band of the coumarin chromophore at a λ_{abs} of 410 nm. On the contrary, the oxazine ring of **1Cl** released from HNTs lumen opens, within 5 min, to generate **1OpH** when the pH of the release medium is lowered to 5.05. Also in this case, a negligible release of the organic molecule from HNTs/**1** nanomaterial is observed. The latter could be crucial for future purposes; the HNTs/**1** nanomaterial, indeed could be potentially used as pH-sensitive probe to monitor the intracellular environment.

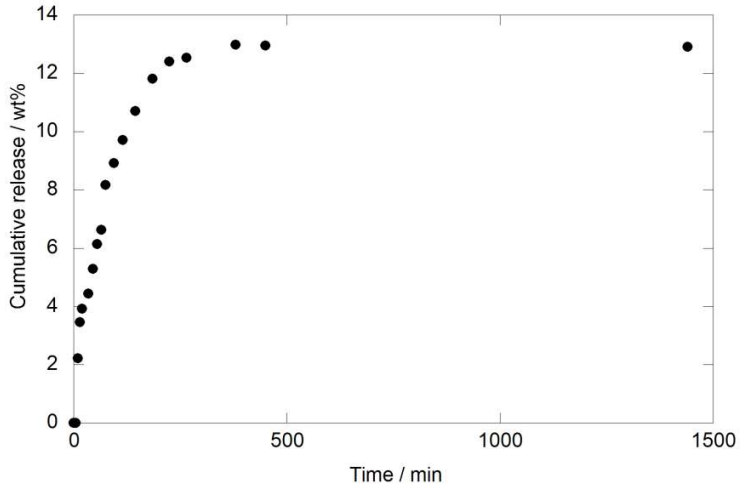

Figure 4. Kinetic release of **1** from HNTs/**1** in a phosphate buffer pH 7.4 at 37 °C (λ_{abs} of 410 nm).

Absorption and Emission Spectroscopies.

The UV-*vis* spectrum of an aqueous dispersion of HNT/**1** nanomaterial is reported in Figure 4. As it is possible to observe, the absorption features of the nanomaterial in water are quite different from the one exhibited by **1** both in organic solvent and aqueous environment[12] and is dominated by an absorption maximum at ca. 595 nm with an additional band around 400 nm. This finding led us to hypothesize that the presence of HNTs induced a confined acidic environment which converts **1Cl** in its open protonated form **1OpH**. The intrinsic acidic nature

of HNTs was indeed proved by recording the UV–*vis* spectrum of a solution of the indicator methylene blue in the presence of HNTs (Figure S4).[18]

Further proof of the presence of **1OpH** species in HNTs/**1** nanomaterial was given by solid-state fluorescence experiments; the spectrum of HNTs/**1** nanomaterial, indeed, shows an emission maximum centered at 660 nm, upon excitation at λ_{ex}= 595 nm (Figure 4).

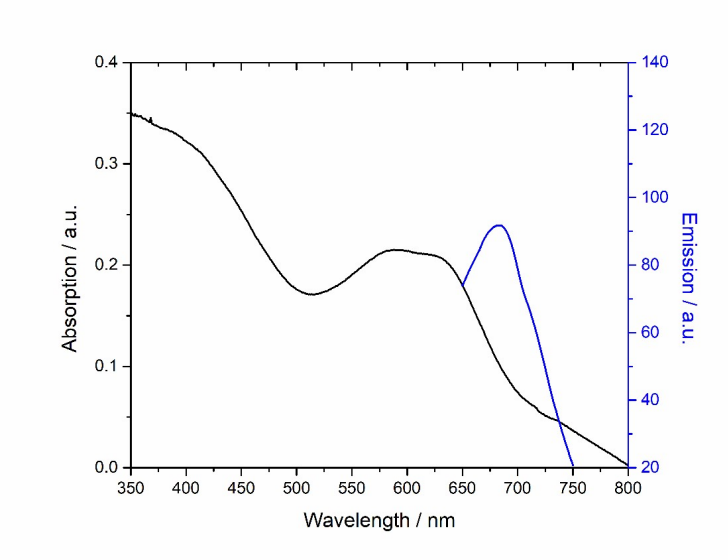

Figure 5. UV-*vis* of an aqueous dispersion of HNTs/**1** (0.16 mg mL $^{-1}$) and solid-state emission spectra of HNTs/**1** (λ_{ex} = 595 nm).

To investigate whether HNTs/**1** could be used as a biological probe, we performed confocal microscopy experiments on three different living cell lines, respectively called hTERT epithelial cells chosen as a model of normal cells, MCF-7 a model of breast cancer chosen as a model of tumor cell lines growing adherent to the support and HL-60R a model of multidrug-resistant acute myeloid leukemia chosen as a model of floating tumor cell lines.

The incubation of all cell lines investigated with HNTs/**1** (10 μM of **1** corresponding to [HNTs/**1**] = 90 μg mL^{-1}) (Figure 6) showed that the nanomaterial can reach the intracellular

compartments of cells on a relatively short time scale (1 h), surrounding cell nuclei. A slight aggregation of nanomaterial indeed was observed in the cytoplasm of the cells, which indicated the heterogeneity of the distribution of nanomaterial in the cytoplasm, in accordance with previous studies.[19] In particular, it is possible to observe a heterogeneous distribution of HNTs/**1** in the cytoplasm, a change in the cellular organization with an increase in the number of cytoplasmic vacuoles and vesicles and a localization of the probe in the perinuclear region. Our results are in according to Liu *et al.*[19] who show that the HNTs signals are partially co-localized with the Golgi and lysosomes apparatus in living cells suggesting that the HNTs have been transported via both organelles. Furthermore, the cytoskeletons, including microtubules and actin filaments, are also involved in the transport pathway of HNTs in tumor cells. In fact, in Figure 5A after 1, 6 and 24 h it is possible to observe the strong red fluorescence of the cytoskeletal structures, especially noticeable in hTERT cells and suggesting that microtubules also participate in cellular trafficking of this nanomaterial.

Interestingly, the hTERT cells incubated with HNTs/**1** can be imaged in two detection channels (Figure 6A) with resolved spectral regions (blue and red emission), indicating that the ring-closed (**1Cl**) and -open (**1OpH**) forms of **1** coexist in aqueous dispersion of the nanomaterial as previously highlighted by spectroscopic measurements.

Moreover after 24 h of incubation, the adsorption of nanomaterials on the membranes and cell uptake did not result in membrane damage. This suggests that HNTs/**1** can be useful as a visualization tool for cancer diagnostics, as already reported elsewhere.[10]

Compared with normal cells, the images of MCF-7 and HL-60R incubated with HNTs/**1** are different (Figure 6B-C). In these cases, indeed, a decrease of blue fluorescence and increase of red one was observed after 6 h of treatment. Furthermore, the observed blue fluorescence does

not always colocalize with the red one, indicating a different distribution inside the same cell which depends on the type of cells used (in adhesion or floating, MCF-7 and HL-60R, respectively; tumoral or normal).

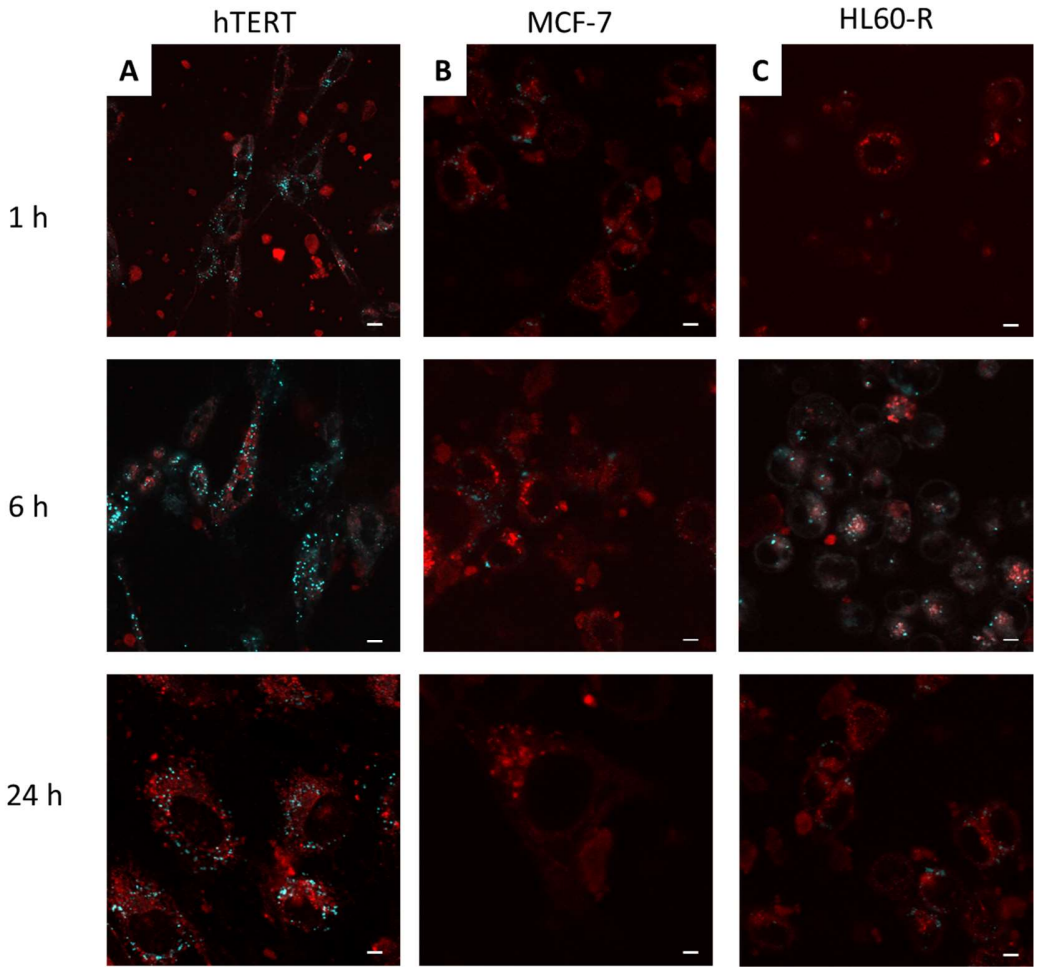

Figure 6. Merged confocal images of hTERT, MCF-7 and HL60-R cell lines incubated with HNTs/**1** (10 μM of **1** corresponding to 90 μg mL^{-1}) at different times. Images were recorded under excitation at 405 nm and 595 nm. Scale bar 10 μm.

CONCLUSIONS

Herein we report the synthesis and characterization of a novel nanomaterial based on the supramolecular assembly of halloysite nanotubes (HNTs) and a switchable halochromic dye for intracellular detection. The dye chosen for this purpose was a fluorescent coumarin chromophore combined with a switchable oxazine (compound **1Cl**) which suffers of insolubility in physiological fluids that limits its application in biological field. After loading of **1Cl** into HNTs, the obtained nanomaterial was thoroughly characterized by several techniques. Morphological investigation by HAADF/STEM measurements coupled with EDX analysis showed that the organic molecules interact with both HNTs surface. The interaction was also investigated by means of some kinetic adsorption experiments. Spectroscopic studies by UV-*vis* and fluorescence measurements highlighted that the intrinsic acidic nature of HNTs allows the opening of the oxazine ring in **1Cl** to give the protonated form **1OpH** and that the two species co-existed in the HNTs based nanomaterial.

Since kinetic release experiments showed that no leaching of the dye from HNTs occurs for at least 24 h, the system is promising as biological probe for tumor detection. Confocal microscopy experiments performed on normal (hTERT) cell lines highlighted the coexistence of the two forms of **1** (the closed **1Cl** and open **1OpH**) as proved by the imaging in two detection channels with resolved spectral regions (blue and red emission). Conversely, the incubation of tumoral cell lines, namely MCF-7 and HL-60R chosen as in adhesion or floating, respectively, model cells with HNTs/**1** showed a decrease of blue fluorescence and increase of red one after 6 h of treatment indicating an opening of the **1Cl**. In conclusion, the nanomaterial reported could be a promising probe for the detection of tumor environment and therefore for application in the diagnostic field.

ASSOCIATED CONTENT

Supporting Information. The following files are available free of charge.

UV-*vis* spectra of **1** with or without HNTs, Kinetic adsorption of **1Cl** on HNTs aqueous dispersion, UV-*vis,* and fluorescence spectra of **1**, UV-*vis* spectra of MB with and without HNTs (word)

AUTHOR INFORMATION

Corresponding Author

*serena.riela@unipa.it

Author Contributions

The manuscript was written through contributions of all authors. All authors have given approval to the final version of the manuscript.

ACKNOWLEDGMENT

The work was carried out in the frame of the PON "AIM: Attrazione e Mobilità Internazionale" No. 1808223-1 project. Confocal measurements were performed at ATeN Center – University of Palermo.

REFERENCES

1. Pawley, J. B., *Handbook of biological confocal microscopy: Third edition*. 2006; p 1-985.
2. Lakowicz, J. R., *Principles of fluorescence spectroscopy*. 2006; p 1-954.
3. Murphy, D. B.; Davidson, M. W., *Fundamentals of Light Microscopy and Electronic Imaging: Second Edition*. 2012.
4. (a) Kobayashi, H.; Ogawa, M.; Alford, R.; Choyke, P. L.; Urano, Y., New Strategies for Fluorescent Probe Design in Medical Diagnostic Imaging. *Chem. Rev.* **2010,** *110* (5), 2620-2640; (b) Specht, E. A.; Braselmann, E.; Palmer, A. E., A Critical and Comparative Review of Fluorescent Tools for Live-Cell Imaging. *Annual Review of Physiology* **2017,** *79* (1), 93-117.

5. (a) Elsabahy, M.; Heo, G. S.; Lim, S.-M.; Sun, G.; Wooley, K. L., Polymeric Nanostructures for Imaging and Therapy. *Chem. Rev.* **2015,** *115* (19), 10967-11011; (b) Swaminathan, S.; Garcia-Amorós, J.; Fraix, A.; Kandoth, N.; Sortino, S.; Raymo, F. M., Photoresponsive polymer nanocarriers with multifunctional cargo. *Chem. Soc. Rev.* **2014,** *43* (12), 4167-4178.
6. Fidecka, K.; Rotiroti, N.; Giacoboni, J.; Cámara, F.; Réfrégiers, M.; Vago, R.; Licandro, E.; Jamme, F., Second-Harmonic Generation of Halloysite Nanotubes for Bioimaging. *ACS Appl. Nano Mater.* **2021,** *4* (5), 4351-4355.
7. (a) Fakhrullina, G. I.; Akhatova, F. S.; Lvov, Y. M.; Fakhrullin, R. F., Toxicity of halloysite clay nanotubes in vivo: a Caenorhabditis elegans study. *Environm. Sci. Nano* **2015,** *2* (1), 54-59; (b) Fan, L.; Zhang, J.; Wang, A., In situ generation of sodium alginate/hydroxyapatite/halloysite nanotubes nanocomposite hydrogel beads as drug-controlled release matrices. *J. Mater. Chem. B* **2013,** *1* (45), 6261-6270; (c) Kryuchkova, M.; Danilushkina, A.; Lvov, Y.; Fakhrullin, R., Evaluation of toxicity of nanoclays and graphene oxide in vivo: a Paramecium caudatum study. *Environm. Sci. Nano* **2016,** *3* (2), 442-452; (d) Wang, X.; Gong, J.; Gui, Z.; Hu, T.; Xu, X., Halloysite nanotubes-induced Al accumulation and oxidative damage in liver of mice after 30-day repeated oral administration. *Environ. Toxicol.* **2018,** *33* (6), 623-630.
8. (a) Lvov, Y.; Aerov, A.; Fakhrullin, R., Clay nanotube encapsulation for functional biocomposites. *Adv. Colloid Interface Sci.* **2014,** *207*, 189-198; (b) Riela, S.; Barattucci, A.; Barreca, D.; Campagna, S.; Cavallaro, G.; Lazzara, G.; Massaro, M.; Pizzolanti, G.; Salerno, T. M. G.; Bonaccorsi, P.; Puntoriero, F., Boosting the properties of a fluorescent dye by encapsulation into halloysite nanotubes. *Dyes and Pigments* **2021,** *187*.
9. Massaro, M.; Barone, G.; Biddeci, G.; Cavallaro, G.; Di Blasi, F.; Lazzara, G.; Nicotra, G.; Spinella, C.; Spinelli, G.; Riela, S., Halloysite nanotubes-carbon dots hybrids multifunctional nanocarrier with positive cell target ability as a potential non-viral vector for oral gene therapy. *J. Colloid Interface Sci.* **2019,** *552*, 236-246.
10. Gorbachevskii, M. V.; Stavitskaya, A. V.; Novikov, A. A.; Fakhrullin, R. F.; Rozhina, E. V.; Naumenko, E. A.; Vinokurov, V. A., Fluorescent gold nanoclusters stabilized on halloysite nanotubes: in vitro study on cytotoxicity. *Appl. Clay Sci.* **2021,** *207*, 106106.
11. Deniz, E.; Sortino, S.; Raymo, F. M., Fluorescence Switching with a Photochromic Auxochrome. *J. Phys. Chem. Lett.* **2010,** *1* (24), 3506-3509.
12. Deniz, E.; Tomasulo, M.; Cusido, J.; Yildiz, I.; Petriella, M.; Bossi, M. L.; Sortino, S.; Raymo, F. M., Photoactivatable Fluorophores for Super-Resolution Imaging Based on Oxazine Auxochromes. *J. Phys. Chem. C* **2012,** *116* (10), 6058-6068.
13. (a) Petriella, M.; Deniz, E.; Swaminathan, S.; Roberti, M. J.; Raymo, F. M.; Bossi, M. L., Superresolution Imaging with Switchable Fluorophores Based on Oxazine Auxochromes. *Photochem. Photobiol.* **2013,** *89* (6), 1391-1398; (b) Cusido, J.; Ragab, S. S.; Thapaliya, E. R.; Swaminathan, S.; Garcia-Amorós, J.; Roberti, M. J.; Araoz, B.; Mazza, M. M. A.; Yamazaki, S.; Scott, A. M.; Raymo, F. M.; Bossi, M. L., A Photochromic Bioconjugate with Photoactivatable Fluorescence for Superresolution Imaging. *J. Phys. Chem. C* **2016,** *120* (23), 12860-12870.
14. Tang, S.; Zhang, Y.; Thapaliya, E. R.; Brown, A. S.; Wilson, J. N.; Raymo, F. M., Highlighting Cancer Cells with Halochromic Switches. *ACS Sensors* **2017,** *2* (1), 92-101.
15. Massaro, M.; Cavallaro, G.; Colletti, C. G.; D'Azzo, G.; Guernelli, S.; Lazzara, G.; Pieraccini, S.; Riela, S., Halloysite nanotubes for efficient loading, stabilization and controlled release of insulin. *J. Colloid Interface Sci.* **2018,** *524*, 156-164.

16. Cavallaro, G.; Grillo, I.; Gradzielski, M.; Lazzara, G., Structure of Hybrid Materials Based on Halloysite Nanotubes Filled with Anionic Surfactants. *J. Phys. Chem. C* **2016,** *120* (25), 13492-13502.
17. Cavallaro, G.; Lazzara, G.; Milioto, S.; Parisi, F.; Evtugyn, V.; Rozhina, E.; Fakhrullin, R., Nanohydrogel Formation within the Halloysite Lumen for Triggered and Sustained Release. *ACS Appl. Mater. Interf.* **2018,** *10* (9), 8265-8273.
18. Marullo, S.; Rizzo, C.; D'Anna, F., Activity of a Heterogeneous Catalyst in Deep Eutectic Solvents: The Case of Carbohydrate Conversion into 5-Hydroxymethylfurfural. *ACS Sustain. Chem. Eng.* **2019,** *7* (15), 13359-13368.
19. Liu, H.; Wang, Z.-G.; Liu, S.-L.; Yao, X.; Chen, Y.; Shen, S.; Wu, Y.; Tian, W., Intracellular pathway of halloysite nanotubes: potential application for antitumor drug delivery. *J. Mater. Sci.* **2019,** *54* (1), 693-704.

SYNOPSIS.

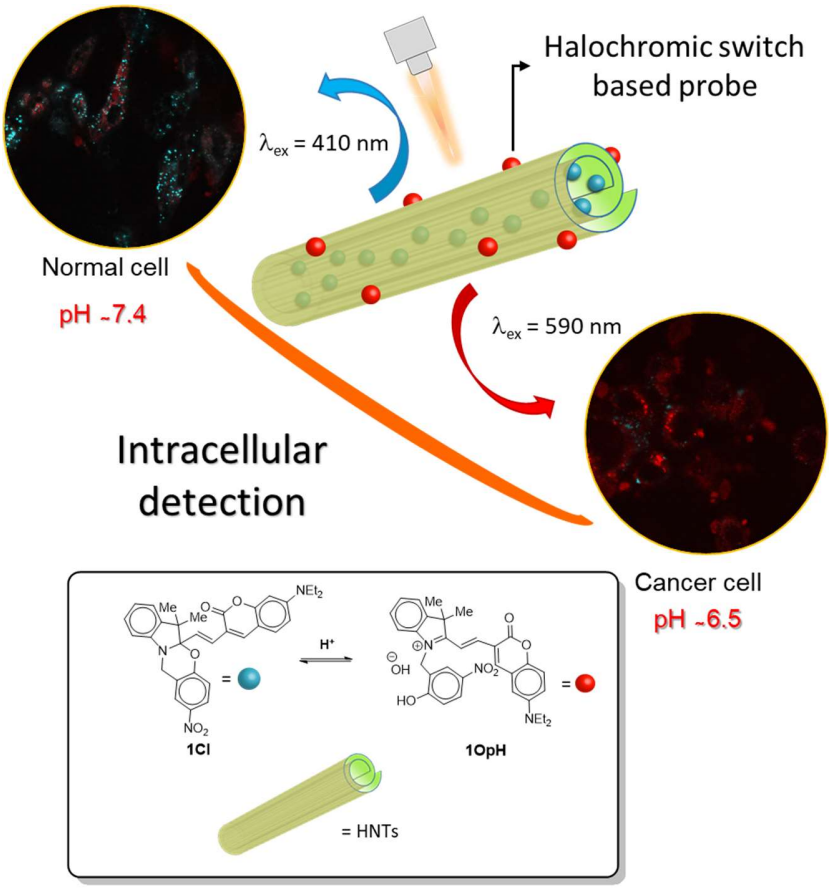
Halochromic switch based probe
λ_{ex} = 410 nm
Normal cell
pH ~7.4
λ_{ex} = 590 nm
Intracellular detection
Cancer cell
pH ~6.5
H+
1Cl
1OpH
= HNTs